

# **CO-sensing properties of a NASICON-based gas sensor attached with Pt mixed with Bi<sub>2</sub>O<sub>3</sub> as a sensing electrode**

Hiroataka TAKEDA, Taro UEDA, Kai KAMADA, Katsuhide MATSUO, Takeo HYODO and Yasuhiro SHIMIZU\*

Graduate School of Engineering, Nagasaki University  
1-14 Bunkyo-machi, Nagasaki 852-8521, Japan

\*Corresponding author:

Yasuhiro SHIMIZU

Graduate School of Engineering, Nagasaki University

1-14 Bunkyo-machi, Nagasaki 852-8521, Japan

TEL: +81-95-819-2642

FAX: +81-95-819-2643

E-mail: [shimizu@nagasaki-u.ac.jp](mailto:shimizu@nagasaki-u.ac.jp)

## Abstract

NASICON ( $\text{Na}_3\text{Zr}_2\text{Si}_2\text{PO}_{12}$ )-based gas sensors capable of detecting various gases ( $\text{CO}_2$ ,  $\text{NO}_2$ ,  $\text{Cl}_2$ , VOC and so on) have so far been developed by many researchers. In this study, planar-type gas sensors using a NASICON disc attached with Pt mixed with  $\text{Bi}_2\text{O}_3$  as a sensing electrode ( $\text{Pt}(n\text{Bi}_2\text{O}_3)$ ,  $n$  ( $0.01\sim 30$ ): the amount of  $\text{Bi}_2\text{O}_3$  addition (wt%)) and Pt as a reference electrode were fabricated, and their sensing properties to CO and  $\text{H}_2$  were examined in the operating temperature range of  $25\sim 300^\circ\text{C}$  in dry and wet air. The sensors obtained were denoted as  $\text{Pt}(n\text{Bi}_2\text{O}_3)/\text{Pt}$ . All  $\text{Pt}(n\text{Bi}_2\text{O}_3)/\text{Pt}$  sensors fabricated responded to CO at all operating temperatures tested, and the magnitude of CO response increased with a decrease in the operating temperature. In addition, the magnitude of CO response largely depended on the additive amounts of  $\text{Bi}_2\text{O}_3$  to the Pt sensing electrode. The increase in the additive amount of  $\text{Bi}_2\text{O}_3$  to the Pt sensing electrode ( $0.01 \leq n \leq 1$ ) enhanced markedly the magnitude of CO response, 90% response time and CO selectivity against  $\text{H}_2$ . The  $\text{Pt}(1\text{Bi}_2\text{O}_3)/\text{Pt}$  sensor showed a linear relationship between the CO response and the logarithm of CO concentration ( $1\sim 3000$  ppm) in dry air at  $25^\circ\text{C}$  and the CO selectivity against  $\text{H}_2$  was enhanced in wet air, in comparison with those observed in dry air. The interfacial layer, which was formed between the NASICON and the  $\text{Pt}(1\text{Bi}_2\text{O}_3)$  electrode, was suggested to play an important role in improving of the CO-sensing properties.

Keywords: gas sensor, carbon monoxide, solid electrolyte, NASICON

## 1. Introduction

Various types of gas sensors (e.g., semiconductor type [1, 2], diode type [3-5], catalytic-combustion type [6] and solid-electrolyte type [7-23]) have been widely investigated and developed to detect various gases such as volatile organic compounds (VOCs) [7, 8], carbon monoxide (CO) [1, 2, 6, 9, 10] and hydrogen (H<sub>2</sub>) [5, 11, 12] under different atmospheres. They have contributed to forestall various serious troubles to human beings, such as sick building syndrome (for VOC), difficulty of breathing (for CO) and explosion accidents (for H<sub>2</sub>). Among them, the solid-electrolyte gas sensors have advantages, since they can detect some kinds of gases selectively and sensitively, by optimization of the composition and microstructure of the gas-sensing electrodes as well as the electrolyte. NASICON (Na<sub>3</sub>Zr<sub>2</sub>Si<sub>2</sub>PO<sub>12</sub>) is well-known as a promising electrolyte which shows relatively high ionic conductivity at low temperatures (e.g.,  $5.2 \times 10^{-2} \text{ S m}^{-1}$  at RT [24]), and thus many efforts have recently directed to developing the NASICON-based gas sensors which can detect various gases, such as SO<sub>2</sub> [13], CO<sub>2</sub> [14-16], NO<sub>2</sub> [17, 18], VOCs, [8], NH<sub>3</sub> [19] and Cl<sub>2</sub> [20]. For example, Obata et al. have demonstrated that a NASICON-based gas sensor using NaNO<sub>2</sub>-Li<sub>2</sub>CO<sub>3</sub> mixed with ITO powders as a sensing electrode material showed stable response to NO<sub>2</sub> without interference of humidity even at RT and the response to NO<sub>2</sub> was proportional to the logarithm of NO<sub>2</sub> concentration [18]. Kida et al. reported that a NASICON-based gas sensor using Bi<sub>2</sub>Cu<sub>0.1</sub>V<sub>0.9</sub>O<sub>5.35</sub> as an electrode material could detect VOCs such as ethanol, formaldehyde and toluene [8]. Lu et al. have reported that a NASICON-based gas sensor using Cr<sub>2</sub>O<sub>3</sub> as a sensing-electrode material showed the high sensitivity to Cl<sub>2</sub> at 300°C [20]. We have also reported that the compositional and morphological optimizations of the Li<sub>2</sub>CO<sub>3</sub>-BaCO<sub>3</sub> auxiliary layer coated onto the sensing electrode of NASICON-based gas sensors were quite effective in improving the CO<sub>2</sub> sensitivity [15, 16]. As described above, different NASICON-based sensors have been already investigated for the detection of various gases, but little effort has been directed to developing NASICON-based CO gas sensors. CO is colorless, odorless and badly hazardous to human health,

and especially it exerts a negative impact on the respiratory system due to its strong associativity with hemoglobin in the blood [25]. Namely, even the small amount of CO (500 ppm) causes various symptoms such as headache, dizziness and nausea, and an increase in the CO concentration more than 1,500 ppm possibly results in death for almost animate beings. Such CO is easily produced from incomplete combustion of fossil fuels used in automobiles, power plants and industrial plants, and therefore high-performance CO sensors, which can detect the low concentration of CO sensitively and selectively, are indispensable for operating them safely and effectively. Recently, we have found that the NASICON-based gas sensor attached with Pt- and/or Au-based electrodes can detect CO at low temperatures and the addition of Bi<sub>2</sub>O<sub>3</sub> powder to the electrodes was the most important factor for the detection of CO [21, 22].

In this study, therefore, the effects of the addition of Bi<sub>2</sub>O<sub>3</sub> powder to a Pt electrode on the CO sensitivity and selectivity of the NASICON-based gas sensors have been investigated in detail at 25~300°C in dry and wet air.

## 2. Experimental

### 2.1 Synthesis of NASICON and Bi<sub>2</sub>O<sub>3</sub> powders

NASICON powder was synthesized from Si(OC<sub>2</sub>H<sub>5</sub>)<sub>4</sub>, Zr(OC<sub>4</sub>H<sub>9</sub>)<sub>4</sub>, PO(OC<sub>4</sub>H<sub>9</sub>)<sub>3</sub> and NaOC<sub>2</sub>H<sub>5</sub> by sol-gel process [15, 16, 26]. The above metal alkoxides in stoichiometric ratios were first dissolved in pure water, together with an equimolar amount of citric acid. The mixture was subjected to heat treatment at 80°C to prepare an organic metal complex, followed by an overnight drying at 120°C. Then, the resultant solid was pyrolyzed at 750°C for 5 h. The precursor obtained was finally calcined in air at 1100°C for 4 h. Bi<sub>2</sub>O<sub>3</sub> powder was synthesized by using the procedure reported in the literature [23] as follows. After Bi(NO<sub>3</sub>)<sub>3</sub>·5H<sub>2</sub>O was fully dissolved in 1.12 M HNO<sub>3</sub> aqueous solution, polyvinyl pyrrolidone was added to the solution as a stabilizing agent and then they were stirred for 15 min. The resultant solution was slowly and continuously dropped into 0.2 M NaOH

solution under constant stirring, until the pH reached 11. After further stirring for 5 min, the resultant suspension was sonicated at 28 kHz for 30 min. The precipitate was centrifuged and washed with pure water for several times. The resultant product was dried at 80°C for 2 h and then annealed at 500°C for 2h.

Crystal structure of these materials synthesized was analyzed by X-ray diffraction (XRD, RINT2100; Rigaku Corp.) with  $\text{CuK}\alpha$  radiation. And their crystallite size was calculated from Scherrer equation. Specific surface area of the  $\text{Bi}_2\text{O}_3$  powder was measured by Brunauer–Emmett–Teller (BET) method using a  $\text{N}_2$  adsorption isotherm (Micromeritics Instruments Corp., Tristar3000), and its microstructure was observed by scanning electron microscopy (SEM; JEOL Ltd., JSM-7500F).

## 2.2 Sensor fabrication

The schematic structure of a NASICON-based planar sensor is shown in Fig. 1. Both Pt paste (Tanaka Corp., TR-7907) mixed with the  $\text{Bi}_2\text{O}_3$  powder and just Pt paste were applied on the same surface of the NASICON disc as a sensing and a counter electrode by screen printing, respectively, and then they were annealed at 700°C for 30 min. The electrode fabricated from the Pt paste mixed with the  $\text{Bi}_2\text{O}_3$  powder was denoted as  $\text{Pt}(n\text{Bi}_2\text{O}_3)$  (the amount of the  $\text{Bi}_2\text{O}_3$  added to Pt ( $n$ ): 0.01~30 wt%), and the sensor obtained was denoted as M/N (M:  $\text{Pt}(n\text{Bi}_2\text{O}_3)$  sensing electrode, N: Pt counter electrode). The secondary electron image (SEI) and backscattered electron image (BEI) of the cross-section of the  $\text{Pt}(n\text{Bi}_2\text{O}_3)/\text{Pt}$  sensors were observed by SEM, and the composition of the electrode/NASICON interface was analyzed with the energy-dispersed spectroscope (EDS; JEOL Ltd., JED-2300) equipped with SEM.

## 2.3 Measurement of gas-sensing properties

Gas response of the sensors obtained was measured to 1~3000 ppm CO and 300 ppm  $\text{H}_2$

balanced with dry or wet (relative humidity: 30 or 60%RH on a basis of the saturated water vapor value at 25°C) air in a flow apparatus (gas-flow rate: 100 cm<sup>3</sup> min<sup>-1</sup>) at 25°C, 100°C and 300°C. The electromotive force (EMF, mV) of the sensors was measured with a digital electrometer as a sensing signal. The magnitude of response was defined as the difference in EMF between in a sample gas and in base air ( $\Delta\text{EMF}_{\text{Gas}}$ , Gas: CO or H<sub>2</sub>). The CO selectivity against H<sub>2</sub> was defined as the ratio of CO response to H<sub>2</sub> response ( $\Delta\text{EMF}_{\text{CO}}/\Delta\text{EMF}_{\text{H}_2}$ ).

### 3. Results and discussion

Figure 2 shows an XRD pattern of the Bi<sub>2</sub>O<sub>3</sub> powder annealed at 500°C for 2 h. Most peaks of the XRD pattern were assigned to monoclinic structure of  $\alpha$ -Bi<sub>2</sub>O<sub>3</sub> (JCPDS No. 71-0465). The average crystallite size calculated from both (1  $\bar{2}$  1) and ( $\bar{2}$  0 2) peaks of the XRD pattern was ca. 70 nm. Figure 3 shows a SEM photograph of the Bi<sub>2</sub>O<sub>3</sub> powder synthesized. Many small particles with a diameter of less than 100 nm, which was similar to the crystallite size, were confirmed in the SEM photograph, and the almost all were largely agglomerated as a relatively large secondary particles (diameter: several hundred nm~ several  $\mu\text{m}$ ). In addition, the specific surface area calculated by the BET method using a N<sub>2</sub> adsorption isotherm was ca. 2.3 m<sup>2</sup> g<sup>-1</sup>. By assuming spherical morphology of all the  $\alpha$ -Bi<sub>2</sub>O<sub>3</sub> crystallites and by using the values of the crystallite size (ca. 70 nm) and the real density of  $\alpha$ -Bi<sub>2</sub>O<sub>3</sub> (8.9 g cm<sup>-3</sup> [27]), the geometric surface area can be calculated to be ca. 9.6 m<sup>2</sup> g<sup>-1</sup>. Since a large amount of the  $\alpha$ -Bi<sub>2</sub>O<sub>3</sub> crystallites were partially sintered and/or contacted each other as shown in Fig. 3, it is considered that all surface of the Bi<sub>2</sub>O<sub>3</sub> crystallites does not contribute to the adsorption of N<sub>2</sub> molecules at 77 K. Thus it is quite reasonable that the measured specific surface area (ca. 2.3 m<sup>2</sup> g<sup>-1</sup>) is smaller than the calculated geometric surface area (ca. 9.6 m<sup>2</sup> g<sup>-1</sup>). SEM photographs of cross-sections of the Pt(*n*Bi<sub>2</sub>O<sub>3</sub>) electrodes of representative Pt(*n*Bi<sub>2</sub>O<sub>3</sub>)/Pt sensors (*n* = 0.01, 1 and 30) were shown in Fig. 4. The thickness of the Pt(0.01/Bi<sub>2</sub>O<sub>3</sub>) electrode was ca. 30  $\mu\text{m}$ , and the thickness and surface roughness of the Pt(*n*Bi<sub>2</sub>O<sub>3</sub>) electrode gradually increased with an

increase in the additive amount of  $\text{Bi}_2\text{O}_3$ , because the viscosity of the  $\text{Bi}_2\text{O}_3$ -mixed Pt paste used for the screen printing increased with an increase in the additive amount ( $n$ ) of  $\text{Bi}_2\text{O}_3$ . From these SEM photographs, the  $\text{Bi}_2\text{O}_3$  added was confirmed to be dispersed almost uniformly in the Pt-based electrode.

Figure 5 shows response transients to 300 ppm CO of representative  $\text{Pt}(n\text{Bi}_2\text{O}_3)/\text{Pt}$  sensors ( $n = 0.01, 1$  and  $30$ ) at 25, 100 and 300°C in dry air. All the sensors showed positive response to CO at all operating temperatures. The  $\text{Pt}(0.01\text{Bi}_2\text{O}_3)/\text{Pt}$  sensor showed small CO response and relatively stable response at 25°C, but response stability of the sensor became extremely low with quite noisy CO response at 100°C, and the sensor showed little CO response at 300°C. On the other hand, the magnitude of CO response of the  $\text{Pt}(1\text{Bi}_2\text{O}_3)/\text{Pt}$  sensor was comparable to that of the  $\text{Pt}(30\text{Bi}_2\text{O}_3)/\text{Pt}$  sensor, and both the  $\text{Pt}(1\text{Bi}_2\text{O}_3)/\text{Pt}$  and  $\text{Pt}(30\text{Bi}_2\text{O}_3)/\text{Pt}$  sensors showed a much larger CO response and more stable response at all the operating temperatures than the  $\text{Pt}(0.01\text{Bi}_2\text{O}_3)/\text{Pt}$  sensor, while the base EMF values in air of both the sensors, which were dependent on the operating temperature, were much lower than that of the  $\text{Pt}(0.01\text{Bi}_2\text{O}_3)/\text{Pt}$  sensor. The magnitude of the CO response of both the sensors was relatively low with overshooting behavior at 300°C, but the magnitude of CO response of both the sensors increased with a decrease in operating temperature, and the sensors showed the largest CO response at 25°C. On the other hand, the response speed of both the sensors decreased with a decrease in operating temperature. The recovery speed of both the sensors also decreased with a decrease in operating temperature, but the EMF values of both the sensors in dry air shifted negatively after the first exposure to CO at 25°C, compared with the initial EMF value in dry air. These results indicated that the addition of  $\text{Bi}_2\text{O}_3$  to Pt electrode was quite effective in improving the CO response of the sensor, but the magnitude of 1st CO response of these sensors was a little bit different from the magnitude of these 2nd and subsequent CO responses. Therefore, CO-sensing properties of other  $\text{Pt}(n\text{Bi}_2\text{O}_3)/\text{Pt}$  sensors with different additive amounts of  $\text{Bi}_2\text{O}_3$  have also been investigated. The variations in the magnitude of 1st and 2nd responses of all the  $\text{Pt}(n\text{Bi}_2\text{O}_3)/\text{Pt}$

sensors to 300 ppm CO in dry air with additive amounts of Bi<sub>2</sub>O<sub>3</sub> to Pt electrode "n" were plotted in Fig. 6. In addition, the variations in the difference in the EMF in dry air between before and after exposure to 300 ppm CO with the additive amounts of Bi<sub>2</sub>O<sub>3</sub> to Pt electrode "n" were shown in Fig. 7. The magnitude of CO response drastically increased with an increase in the additive amount of Bi<sub>2</sub>O<sub>3</sub> to Pt electrode "n" up to ca. 1 wt% at all the operating temperatures. However, further increase in the additive amount of Bi<sub>2</sub>O<sub>3</sub> ( $n \geq 1$ ) was almost ineffective in further improving the magnitude of CO response. In addition, the magnitude of CO response largely increased with a decrease in the operating temperature. On the other hand, all the Pt(*n*Bi<sub>2</sub>O<sub>3</sub>)/Pt sensors showed the relatively stable EMF values in dry air, but very small CO response at 300°C, as shown in Fig. 7. On the other hand, both the magnitude of the difference in EMF of the sensors in dry air between before and after the exposure to 300 ppm CO and the direction of the shift in EMF varied irregularly by the additive amounts of Bi<sub>2</sub>O<sub>3</sub> at 100°C. The EMF difference of the sensors negatively increased with an increase in the additive amount of Bi<sub>2</sub>O<sub>3</sub> at 25°C (see Fig. 7), whereas the EMF values in CO atmosphere remained unchanged by successive exposure to CO (see Fig. 5). Therefore, the Pt(*n*Bi<sub>2</sub>O<sub>3</sub>)/Pt sensors showed slightly larger 2nd CO response than 1st CO response at 25°C, as shown in Fig. 6. In addition, 90% response and recovery times of all the Pt(*n*Bi<sub>2</sub>O<sub>3</sub>)/Pt sensors to 300 ppm CO on the first exposure in dry air is plotted against the additive amounts of Bi<sub>2</sub>O<sub>3</sub> to Pt electrode "n" in Fig. 8. The Pt(0.01Bi<sub>2</sub>O<sub>3</sub>)/Pt sensor showed extremely long response time, especially at 25°C and 100°C, but the response time also largely shortened with an increase in the additive amount of Bi<sub>2</sub>O<sub>3</sub> up to ca. 1 wt%, as was observed with the case of the variations in CO response (see Fig. 6). These results apparently indicate that the 1 wt% Bi<sub>2</sub>O<sub>3</sub> addition is enough for improving both the magnitude of CO response and the response speed. However, the Bi<sub>2</sub>O<sub>3</sub> addition did not have a positive effect on the recovery speed as shown in Fig. 8(b).

H<sub>2</sub>-sensing properties of the Pt(*n*Bi<sub>2</sub>O<sub>3</sub>)/Pt sensors have also been investigated in this study to evaluate the CO selectivity against H<sub>2</sub>. Figure 9 shows response transients to both 300 ppm CO and

300 ppm H<sub>2</sub> of representative sensors, Pt(*I*Bi<sub>2</sub>O<sub>3</sub>)/Pt and Pt(*0.0I*Bi<sub>2</sub>O<sub>3</sub>)/Pt, at 25, 100 and 300°C in dry air. The Pt(*0.0I*Bi<sub>2</sub>O<sub>3</sub>)/Pt sensor showed small H<sub>2</sub> response with unstable small CO response transients as mentioned above, at all the operating temperatures. On the other hand, the Pt(*I*Bi<sub>2</sub>O<sub>3</sub>)/Pt sensor showed relatively large H<sub>2</sub> response in comparison with that of the Pt(*0.0I*Bi<sub>2</sub>O<sub>3</sub>)/Pt sensor. In addition, the magnitude of H<sub>2</sub> response of the Pt(*I*Bi<sub>2</sub>O<sub>3</sub>)/Pt sensor was comparable to the magnitude of CO response at 300°C. However, the CO response the Pt(*I*Bi<sub>2</sub>O<sub>3</sub>)/Pt sensor was much larger than the H<sub>2</sub> response at 25°C, as the CO response increased and the H<sub>2</sub> response decreased with a decrease in the operating temperature, respectively. Response transients to both 300 ppm CO and 300 ppm H<sub>2</sub> of other typical Pt(*n*Bi<sub>2</sub>O<sub>3</sub>)/Pt sensors were also investigated, and the variations in the H<sub>2</sub> response and CO selectivity against H<sub>2</sub> of all the Pt(*n*Bi<sub>2</sub>O<sub>3</sub>)/Pt sensors with the additive amounts of Bi<sub>2</sub>O<sub>3</sub> to Pt electrode were shown in Fig. 10. The magnitude of H<sub>2</sub> response gradually increased with an increase in the additive amount of Bi<sub>2</sub>O<sub>3</sub> up to *n* = 0.1 at all the operating temperatures, but the H<sub>2</sub> response remained almost unchanged at 25 and 300°C or decreased at 100°C by further increase in the additive amount of Bi<sub>2</sub>O<sub>3</sub> (*n* ≥ 1). The magnitude of H<sub>2</sub> response tended to be small at low operating temperature, and thus the CO selectivity against H<sub>2</sub> of the Pt(*n*Bi<sub>2</sub>O<sub>3</sub>)/Pt sensors improved at 25°C. In addition, the CO selectivity against H<sub>2</sub> improved with an increase in the additive amount of Bi<sub>2</sub>O<sub>3</sub> only at 25°C, and the Pt(30Bi<sub>2</sub>O<sub>3</sub>)/Pt sensor showed the largest CO selectivity against H<sub>2</sub> at 25°C among them. Thus, it was revealed that the addition of Bi<sub>2</sub>O<sub>3</sub> to the Pt electrode was also quite effective in improving the CO selectivity against H<sub>2</sub> only at 25°C.

Figure 11 shows concentration dependence of the CO response of the Pt(*I*Bi<sub>2</sub>O<sub>3</sub>)/Pt sensor in dry air at 25, 100 and 300°C, and Fig. 12 shows response transients to 1 ppm CO of the sensor at 25, 100 and 300°C in dry air. The sensor showed an almost linear relationship between the CO response and the logarithm of CO concentration at all the operating temperatures, and the slope, namely CO sensitivity, increased with a decrease in the operating temperature. The Pt(*I*Bi<sub>2</sub>O<sub>3</sub>)/Pt sensor showed relatively large response even to 1 ppm CO (ca. 17 mV at both 25 and 100°C) with a slightly slow

response speed at 25 and 100°C, while it showed smaller CO response at 300°C (ca. 4 mV) after too large overshooting (ca. +50 mV) upon exposure to CO. This response properties sufficiently promise that the Pt(*I*Bi<sub>2</sub>O<sub>3</sub>)/Pt sensor can easily detect a low concentration of CO (< 1 ppm, at least) at low temperatures.

Figure 13 shows response transients of the Pt(*I*Bi<sub>2</sub>O<sub>3</sub>)/Pt sensor to 300 ppm CO and H<sub>2</sub> in dry and wet air, and variation in the CO selectivity against H<sub>2</sub> with relative humidity in air at 25°C. In wet atmosphere the CO response decreased in comparison with that in dry air, but the magnitude of CO response at 30%RH was comparable to that at 60%RH. In addition, the response and recovery speeds in wet air were also slower than those in dry air. As was confirmed again, the EMF value of the sensor in dry air shifted negatively after the first exposure to CO at 25°C. In wet air, however, the EMF values after the first exposure to CO remained almost unchanged. Furthermore, the sensor showed almost no H<sub>2</sub> response in wet air. Therefore, the CO selectivity against H<sub>2</sub> in wet air was much larger than that in dry air in spite of the small CO response in wet air, as shown in Fig. 13(b). Thus, it was confirmed that the Pt(*n*Bi<sub>2</sub>O<sub>3</sub>)/Pt sensor showed moderate CO response as well as excellent CO selectively against H<sub>2</sub> in wet air at 25°C.

It is well-known that solid-electrolyte gas sensors generally show negative EMF responses to reducing gases, such as CO, H<sub>2</sub> and various inflammable gases [8, 12], but the EMF value of the present planar-type Pt(*n*Bi<sub>2</sub>O<sub>3</sub>)/Pt sensors positively shifted upon exposure to CO, as shown in Figs. 5, 9, 12 and 13. As both the sensing and counter electrodes of the Pt(*n*Bi<sub>2</sub>O<sub>3</sub>)/Pt sensors are attached on the same side of the NASICON pellet and they are always exposed to the same gaseous atmosphere, the change in potential of both the electrodes by the addition of CO into the gaseous atmosphere absolutely influence on the EMF value of the sensors. In order to investigate the influence of the potential change of the counter Pt electrode upon exposure to CO, therefore, a solid-electrolyte sensor which is attached with a sensing electrode (Pt(*I*5Bi<sub>2</sub>O<sub>3</sub>) or Pt) and a counter Pt electrode on the front and back of a NASICON pellet, respectively, was fabricated as shown in Fig.

14, and the EMF response of the sensor to 300 ppm CO in dry air was investigated, while the counter electrode was constantly exposed to a reference dry air [8]. In fabricating the sensor, an Al<sub>2</sub>O<sub>3</sub>-based inorganic adhesive (TOAGOSEI Co., Ltd.; Aron Ceramic D) was used in order to adhere the NASICON disc with the alumina tube tightly. This type of the sensor was denoted as SE-Pt (SE: sensing electrode, Pt(*15*Bi<sub>2</sub>O<sub>3</sub>) or Pt). Figure 15 shows response transients to 300 ppm CO of the Pt(*15*Bi<sub>2</sub>O<sub>3</sub>)-Pt and Pt-Pt sensors in dry air at 25°C. The Pt(*15*Bi<sub>2</sub>O<sub>3</sub>)-Pt sensor showed a positive EMF response to CO, while the Pt-Pt sensor showed a negative EMF response to CO. As the EMF value of the planar-type Pt(*n*Bi<sub>2</sub>O<sub>3</sub>)/Pt sensors is defined as the difference in electrode potential between the Pt(*n*Bi<sub>2</sub>O<sub>3</sub>) sensing electrode and the Pt counter electrode, it was confirmed that the large magnitude of positive CO response of the planar-type Pt(*n*Bi<sub>2</sub>O<sub>3</sub>)/Pt sensors originated from both the positive CO response of the Pt(*15*Bi<sub>2</sub>O<sub>3</sub>) and the negative CO response of the Pt electrode. We also speculate the sensing mechanism of the present sensor can also be explained by the mixed-potential theory. Several reports concluded that the response of the mixed-potential type sensors can be generated at the equal magnitude of the cathodic current to the anodic one under the conditions of the occurrence of more than two reactions, i.e. electrochemical reduction and oxidation of chemicals including a target gas [8, 19, 20].

To get information on an accurate redox reaction responsible for the CO response, the morphology and composition of the interface between the Pt(*15*Bi<sub>2</sub>O<sub>3</sub>) electrode and NASICON in the Pt(*15*Bi<sub>2</sub>O<sub>3</sub>)/Pt sensor were investigated by SEM and EDS. Cross-sectional SEI and BEI images of the Pt(*15*Bi<sub>2</sub>O<sub>3</sub>)/NASICON interface of the Pt(*15*Bi<sub>2</sub>O<sub>3</sub>)/Pt sensor are shown in Fig. 16. It was clearly observed that the intermediate layer (ca. 1.1~1.8 μm in thickness) was formed between the Pt(*15*Bi<sub>2</sub>O<sub>3</sub>) electrode and the NASICON pellet. The composition of the intermediate layer, which was analyzed with EDS equipped with SEM, was listed in Table 1, together with that of the NASICON pellet. The existence of large amounts of Bi and Pt components was confirmed at the intermediate layer by EDS, in addition to constituents of NASICON (Na, Si, P and Zr). To confirm

the reactivity of  $\text{Bi}_2\text{O}_3$  with NASICON, the NASICON powder mixed with the  $\text{Bi}_2\text{O}_3$  powder was annealed at  $700^\circ\text{C}$  for 30 min, and then the crystal structure was analyzed by XRD, as shown in Fig. 17. Most of the XRD peaks were assigned to either NASICON,  $\text{Bi}_2\text{SiO}_5$  or  $\text{BiPO}_4$ . Recently, it is reported that such an interfacial layer formed between the sensing electrode and solid electrolyte has an important role in improving gas-sensing properties as well as long-term stability of solid-electrolyte gas sensors. For example, Pasierb et al. reported that the formation of the interfacial layer by the reaction of NASICON and  $\text{Li}_2\text{CO}_3/\text{BaCO}_3$  carbonate improved the long-term stability of the sensor performance [28]. Kida et al. reported that the interfacial layer formed by the reaction of NASICON electrolyte with the sensing  $\text{BiCuVO}_x$ -based electrode worked as an oxidation catalyst for various VOCs in improving the VOC-sensing properties [8]. Also in the present study, therefore, we can speculate that the new phases,  $\text{Bi}_2\text{SiO}_5$  and  $\text{BiPO}_4$ , which were produced by the reaction with NASICON and  $\alpha\text{-Bi}_2\text{O}_3$  may greatly contribute to the large CO response as well as the long-term stability of the  $\text{Pt}(n\text{Bi}_2\text{O}_3)/\text{Pt}$  sensors. However, the accurate redox reaction during the CO sensing has not been established yet. A more detailed CO-sensing mechanism of the  $\text{Pt}(n\text{Bi}_2\text{O}_3)/\text{Pt}$  sensors are currently under investigation.

#### 4. Conclusions

CO-sensing properties of  $\text{Pt}(n\text{Bi}_2\text{O}_3)/\text{Pt}$  sensors ( $0.01 \leq n \leq 30$ ) were examined in air at 25, 100 and  $300^\circ\text{C}$ . All the sensors showed relatively large CO response at lower operating temperatures. In addition, the magnitude of CO response, the response speed of the sensors and CO selectivity against  $\text{H}_2$  in dry air at  $25^\circ\text{C}$  largely enhanced with an increase in the amount of  $\text{Bi}_2\text{O}_3$  added to the Pt electrode. The  $\text{Pt}(1\text{Bi}_2\text{O}_3)/\text{Pt}$  sensor showed a linear relationship between the CO response and the logarithm of CO concentration (1~3000 ppm) in dry air at  $25^\circ\text{C}$ . In wet air the CO selectivity of the  $\text{Pt}(1\text{Bi}_2\text{O}_3)/\text{Pt}$  sensor against  $\text{H}_2$  was enhanced, but the magnitude of the CO response and the response speed decreased, in comparison with those observed in dry air. The interfacial layer, which

was formed between the NASICON and the Pt( $\text{Bi}_2\text{O}_3$ )/Pt electrode, was suggested to play an important role in improving of the CO-sensing properties.

## References

1. H. Torvela, J. Huusko, V. Lantto, *Sens. Actuators B*, 3 (1991) 479-484.
2. S. Habibzadeh, A. Khodadadi, Y. Mortazavi, *Sens. Actuators B*, 144 (2010) 131-138.
3. F. Juang, Y. Fang, Y. Chiang, T. Chou, C. Lin, C. Lin, *Sens. Actuators B*, 156 (2011) 338-342.
4. Y. Gurbuz, W. P. Kang, J. L. Davidson, D. V. Kerns, *Sens. Actuators B*, 56 (1999) 151-154.
5. G. Yamamoto, T. Yamashita, K. Matsuo, T. Hyodo, Y. Shimizu, *Sens. Actuators B*, 183 (2013) 253-264.
6. D. Nagai, T. Nakashima, M. Nishibori, T. Itoh, N. Izu, W. Shin, *Sens. Actuators B*, 182 (2013) 789-794.
7. T. Sato, V. Plashnitsa, M. Utiyama, N. Miura, *Electrochem. Commun.*, 12 (2010) 524-526.
8. T. Kida, N. Morinaga, S. Kishi, K. An, K. Sim, B. Chae, J. Kim, B. Ryu, K. Shimano, *Electrochim. Acta*, 56 (2011) 7484-7490.
9. V. Plashnitsa, S. Anggraini, N. Miura, *Electrochem. Commun.*, 13 (2011) 444-446.
10. S. Anggraini, V. Plashnitsa, P. Elumalai, M. Breedon, *Sens. Actuators B*, 160 (2011) 1273-1281.
11. M. Yamaguchi, S. Anggraini, Y. Fujio, M. Breedon, V. Plashnitsa, *Electrochimica Acta*, 76 (2012) 152-158.
12. L. Xishuang, L. Jianguo, G. Yingzhou, Z. Han, L. Fengmin, L. Geyu, *Sens. Actuators B*, 185 (2013) 77-83.
13. X. Liang, T. Zhong, B. Quan, B. Wang, H. Guan, *Sens. Actuators B*, 134 (2008) 25-30.
14. H. Dang, X. Guo, *Sens. Actuators B*, 178 (2013) 163-168.
15. T. Hyodo, T. Furuno, S. Kumazawa, Y. Shimizu, M. Egashira, *Sensors and Materials*, 19(6) (2007) 365-376.
16. M. Morio, T. Hyodo, Y. Shimizu, M. Egashira, *Sensors and Actuators B*, 139 (2009) 563-569.
17. N. Miura, J. Wang, P. Elumalai, T. Ueda, D. Terada, M. Hasei, *Sens. Actuators B*, 154(8) (2007) J246-J252.

18. K. Obata, S. Matsushima, *Sens. Actuators B*, 130 (2008) 269-276.
19. X. Liang, T. Zhong, H. Guan, F. Liu, G. Lu, B. Quan, *Sens. Actuators B*, 136 (2009) 479-483.
20. Z. Han, L. Jianguo, Z. Houbo, L. Xishuang, Y. Chengguo, D. Quan, Z. Jie, L. Geyu, *Sens. Actuators B*, 180 (2013) 66-70.
21. J. Iwabuchi, T. Hyodo, Y. Simizu, *Chemical Sensors*, 27 (2011) 40-42.
22. H. Takeda, T. Hyodo, Y. Shimizu, *Chemical Sensors*, 29 (2013) 82-84.
23. N. Pugazhenthiran, P. Sathishkumar, S. Murugesan, S. Anandan, *Chem. Eng. J.*, 168 (2011) 1227-1233.
24. O. Bohnke, S. Ronchetti, D. Mazza, *Solid State Ionics*, 122 (1999) 127-136.
25. C. Shi, H. Qin, M. Zhao, X. Wang, L. Li, J. Hu, *Sens. Actuators B*, 190 (2014) 25-31.
26. Y. L. Huang, A. Caneiro, M. Attari, P. Fabry, *Thin Solid Films*, 196(2) (1991) 283-294.
27. D. L. Perry, *Handbook of Inorganic Compounds*, Second Edition, CRC Press (2011) 68-69.
28. P. Pasierb, S. Komornicki, S. Kozinski, R. Gajerski, M. Rekas, *Sens. Actuators B*, 101 (2004) 47-56.

## Figure captions

- Fig. 1** Schematic structure of a NASICON-based planar gas sensor.
- Fig. 2** XRD pattern of the  $\text{Bi}_2\text{O}_3$  powder annealed at  $500^\circ\text{C}$  for 2 h.
- Fig. 3** SEM photograph of the  $\text{Bi}_2\text{O}_3$  powder annealed at  $500^\circ\text{C}$  for 2 h.
- Fig. 4** SEM photographs of cross-sections of  $\text{Pt}(n\text{Bi}_2\text{O}_3)$  electrodes of  $\text{Pt}(n\text{Bi}_2\text{O}_3)/\text{Pt}$  sensors ( $n = 0.01, 1$  and  $30$ ).
- Fig. 5** Response transients to 300 ppm CO of  $\text{Pt}(n\text{Bi}_2\text{O}_3)/\text{Pt}$  sensors ( $n = 0.01, 1$  and  $30$ ) at 25, 100 and  $300^\circ\text{C}$  in dry air.
- Fig. 6** Variations in the magnitude of 1st and 2nd responses of all  $\text{Pt}(n\text{Bi}_2\text{O}_3)/\text{Pt}$  sensors to 300 ppm CO in dry air with the additive amounts of  $\text{Bi}_2\text{O}_3$  to the Pt electrode.
- Fig. 7** Variations in the difference in EMF in dry air between before and after exposure to 300 ppm CO with the additive amounts of  $\text{Bi}_2\text{O}_3$  to the Pt electrode.
- Fig. 8** Variations in 90% response and recovery time of all  $\text{Pt}(n\text{Bi}_2\text{O}_3)/\text{Pt}$  sensors on the 1st exposure to 300 ppm CO in dry air with the additive amounts of  $\text{Bi}_2\text{O}_3$  to the Pt electrode.
- Fig. 9** Response transients to 300 ppm CO and 300 ppm  $\text{H}_2$  of the  $\text{Pt}(0.01\text{Bi}_2\text{O}_3)/\text{Pt}$  and  $\text{Pt}(1\text{Bi}_2\text{O}_3)/\text{Pt}$  sensors at 25, 100 and  $300^\circ\text{C}$  in dry air.
- Fig. 10** Variations in (a)  $\text{H}_2$  response and (b) CO selectivity against  $\text{H}_2$  of all  $\text{Pt}(n\text{Bi}_2\text{O}_3)/\text{Pt}$  sensors with the additive amounts of  $\text{Bi}_2\text{O}_3$  to the Pt electrode.
- Fig. 11** Dependence of the CO response of the  $\text{Pt}(1\text{Bi}_2\text{O}_3)/\text{Pt}$  sensor on the CO concentration in dry air at 25, 100 and  $300^\circ\text{C}$ .
- Fig. 12** Response transients to 1 ppm CO of the  $\text{Pt}(1\text{Bi}_2\text{O}_3)/\text{Pt}$  sensor at 25, 100 and  $300^\circ\text{C}$  in dry air.
- Fig. 13** (a) Response transients of the  $\text{Pt}(1\text{Bi}_2\text{O}_3)/\text{Pt}$  sensor to 300 ppm CO and  $\text{H}_2$  in dry and wet air and (b) variation in CO selectivity against  $\text{H}_2$  of the  $\text{Pt}(1\text{Bi}_2\text{O}_3)/\text{Pt}$  sensor with relative humidity in air at  $25^\circ\text{C}$ .

**Fig. 14** Schematic drawing of a NASICON-based sensor attached with a sensing electrode and a counter Pt electrode on the front and back of a NASICON pellet, respectively.

**Fig. 15** Response transients to 300 ppm CO of the Pt( $15\text{Bi}_2\text{O}_3$ )-Pt and (b) Pt-Pt sensors at 25°C in dry air.

**Fig. 16** SEM photographs ((a) SEI and (b) BEI) of the cross-section of the Pt( $15\text{Bi}_2\text{O}_3$ )/NASICON interface of the Pt( $15\text{Bi}_2\text{O}_3$ )/Pt sensor.

**Fig. 17** XRD pattern of the mixture of NASICON and  $\text{Bi}_2\text{O}_3$  powders after annealing at 700°C for 30 min.

Table 1 Composition of NASICON and the intermediate layer formed between Pt( $15\text{Bi}_2\text{O}_3$ ) electrode and NASICON.

Sample	Elements (mol%)					
	Na	Si	P	Zr	Pt	Bi
<b>NASICON</b>	32	35	15	18	-	-
<b>Interfacial layer</b>	4.2	5.5	23.3	16	23	28

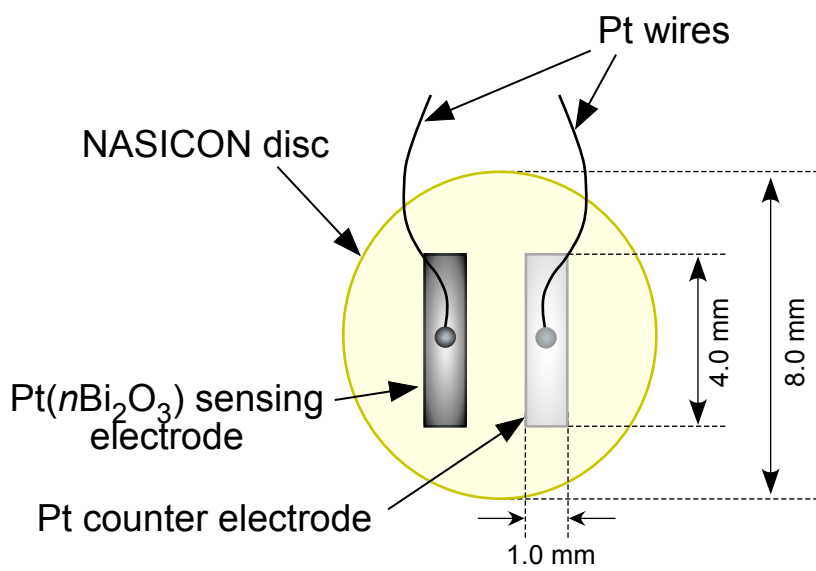


Fig. 1 Takeda et al.

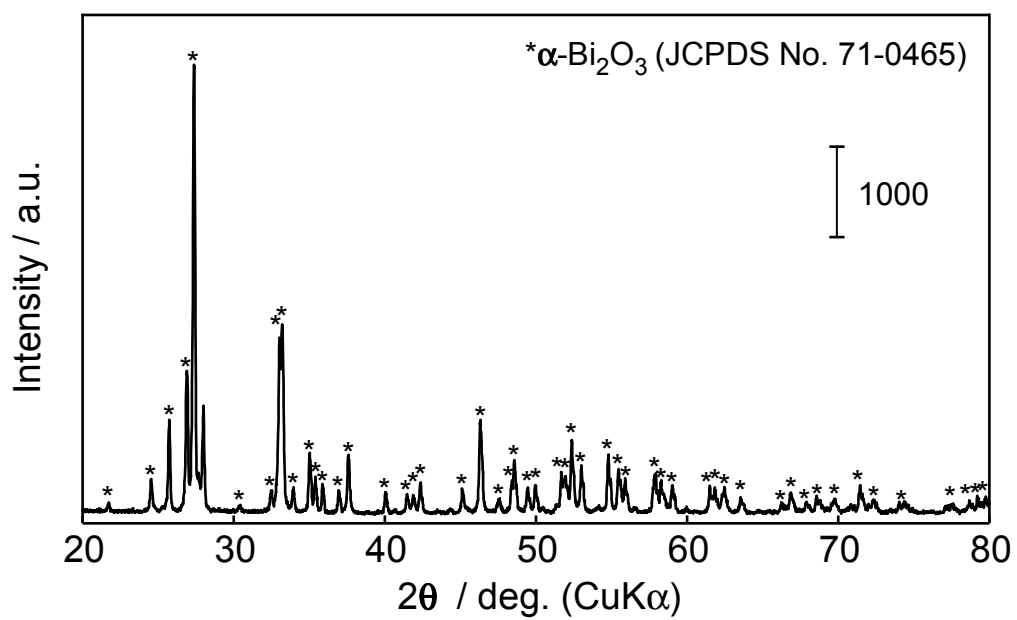


Fig. 2 Takeda et al.

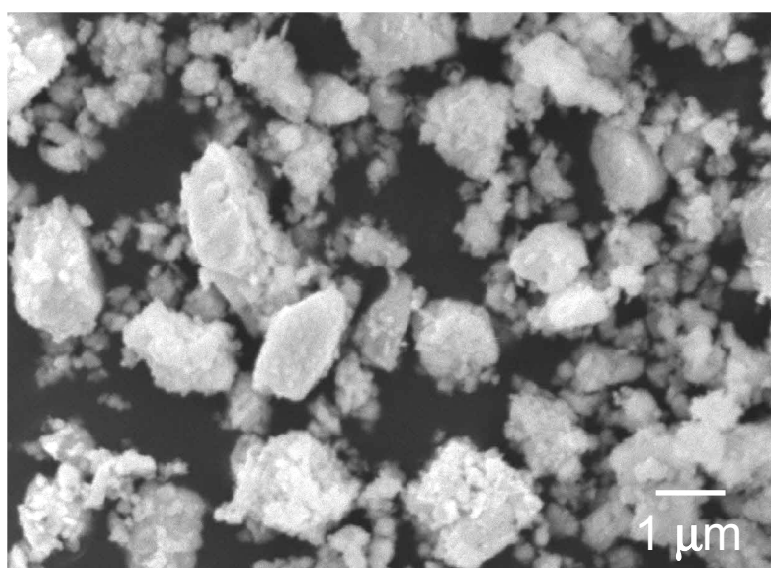


Fig. 3 Takeda et al.

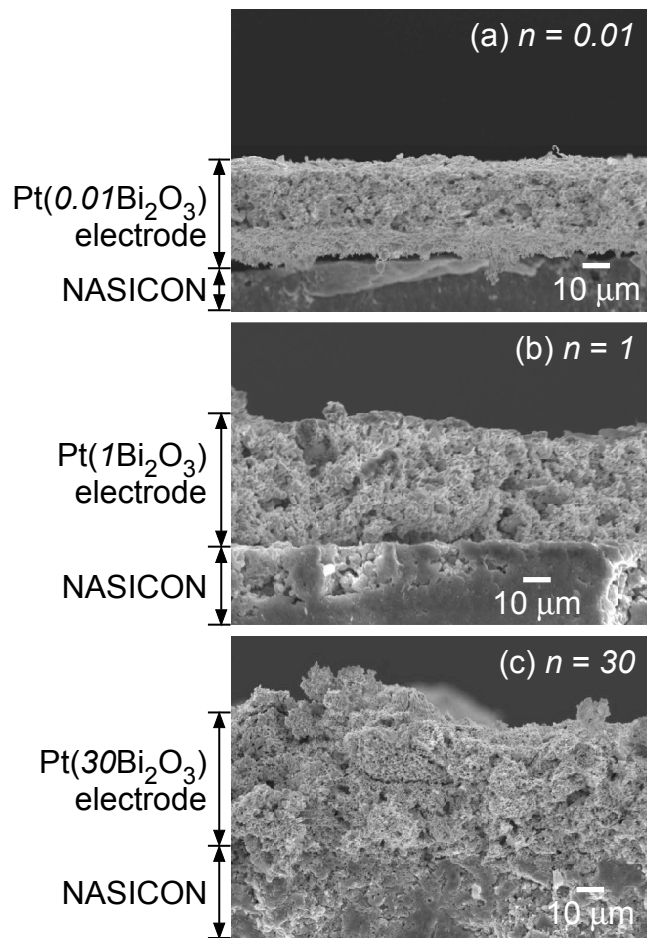


Fig. 4 Takeda et al.

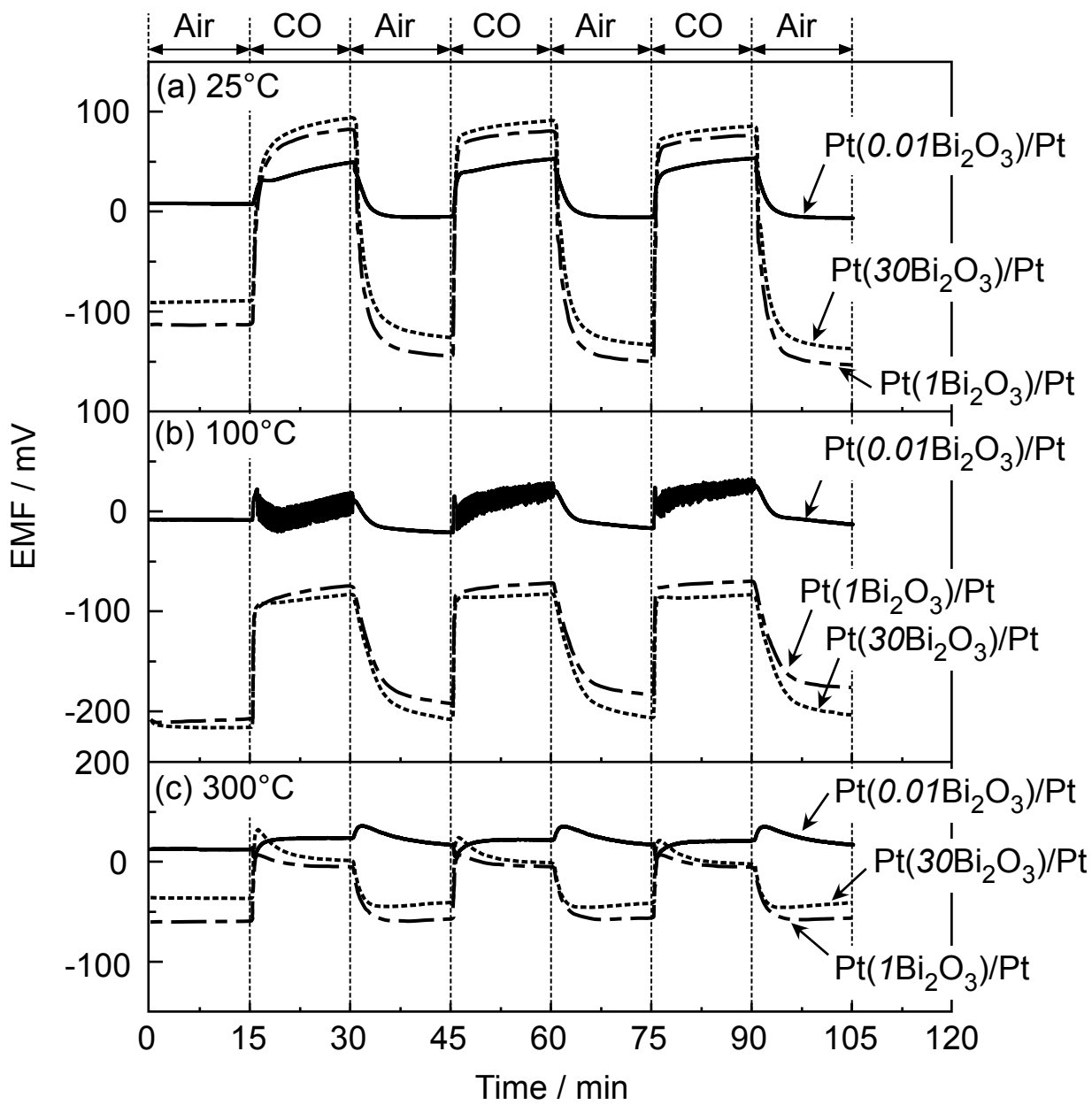


Fig. 5 Takeda et al.

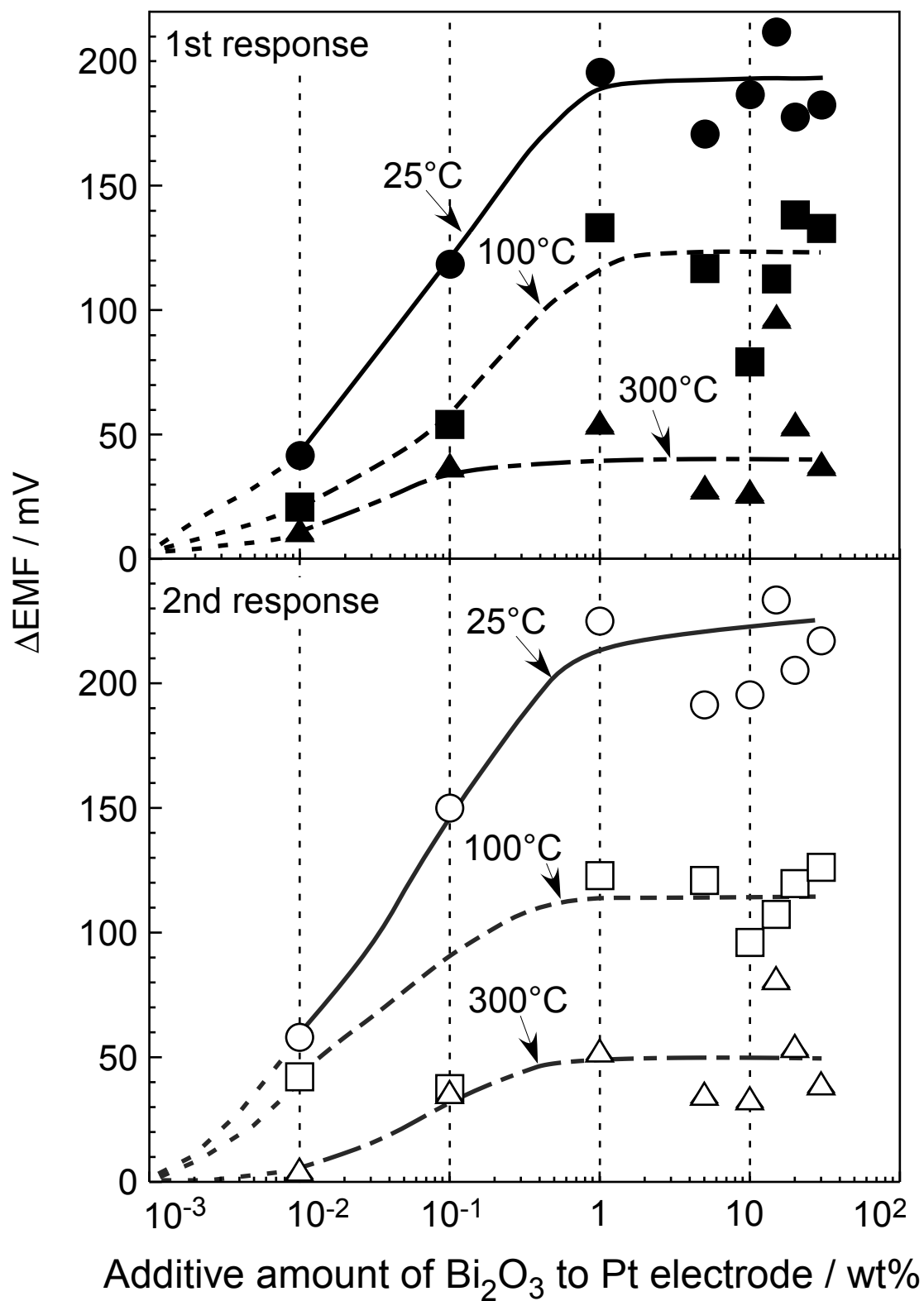


Fig. 6 Takeda et al.

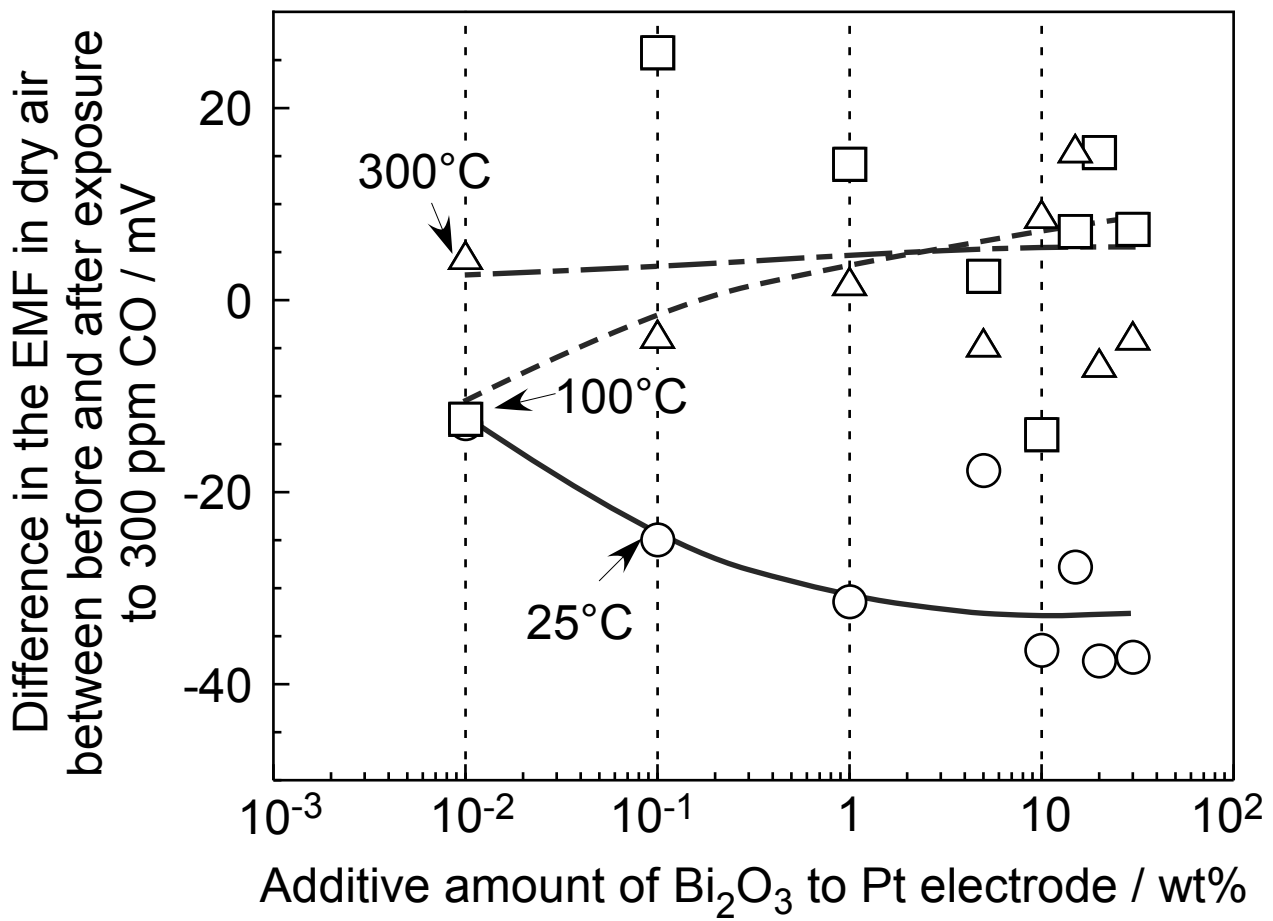


Fig. 7 Takeda et al.

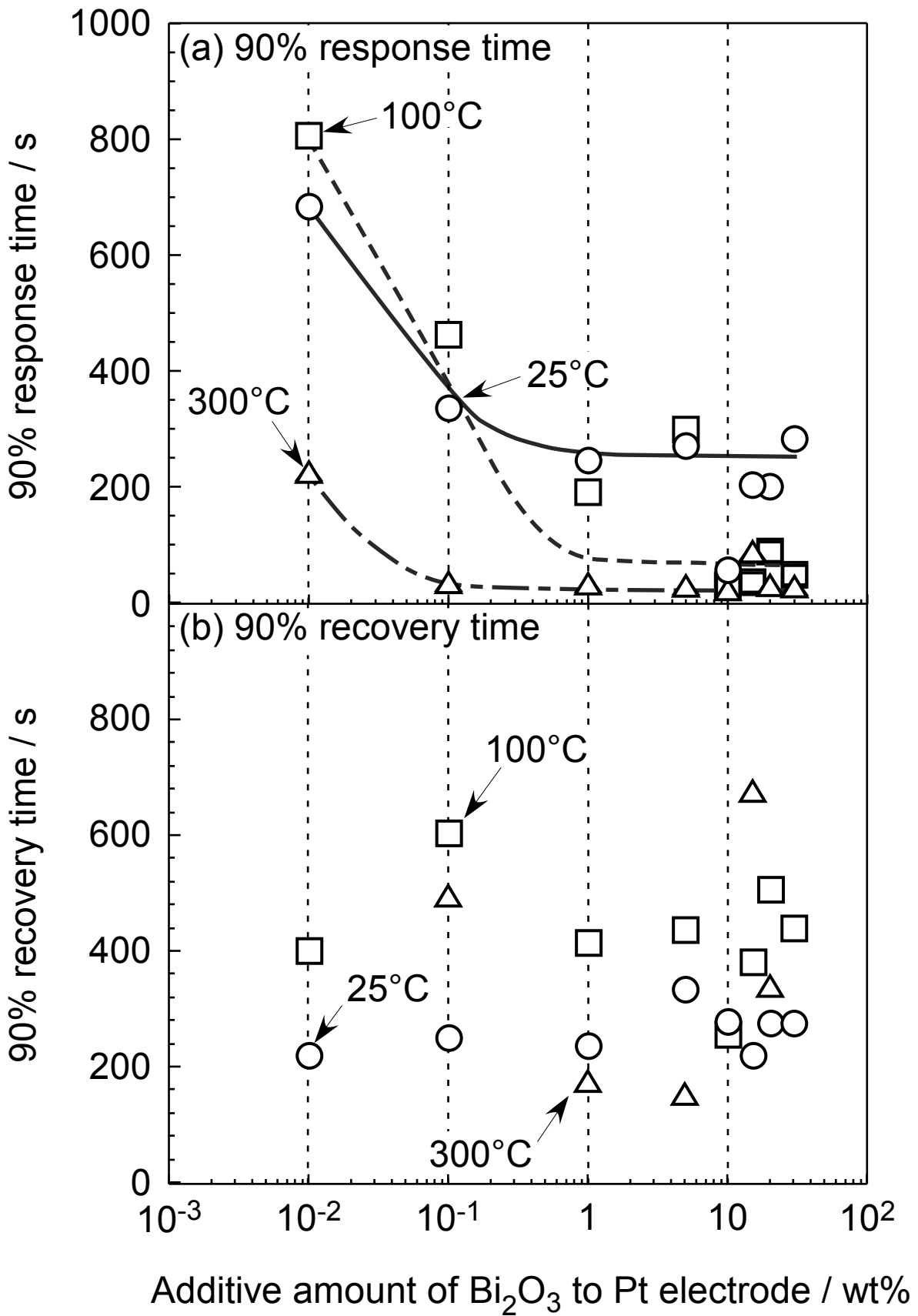


Fig. 8 Takeda et al.

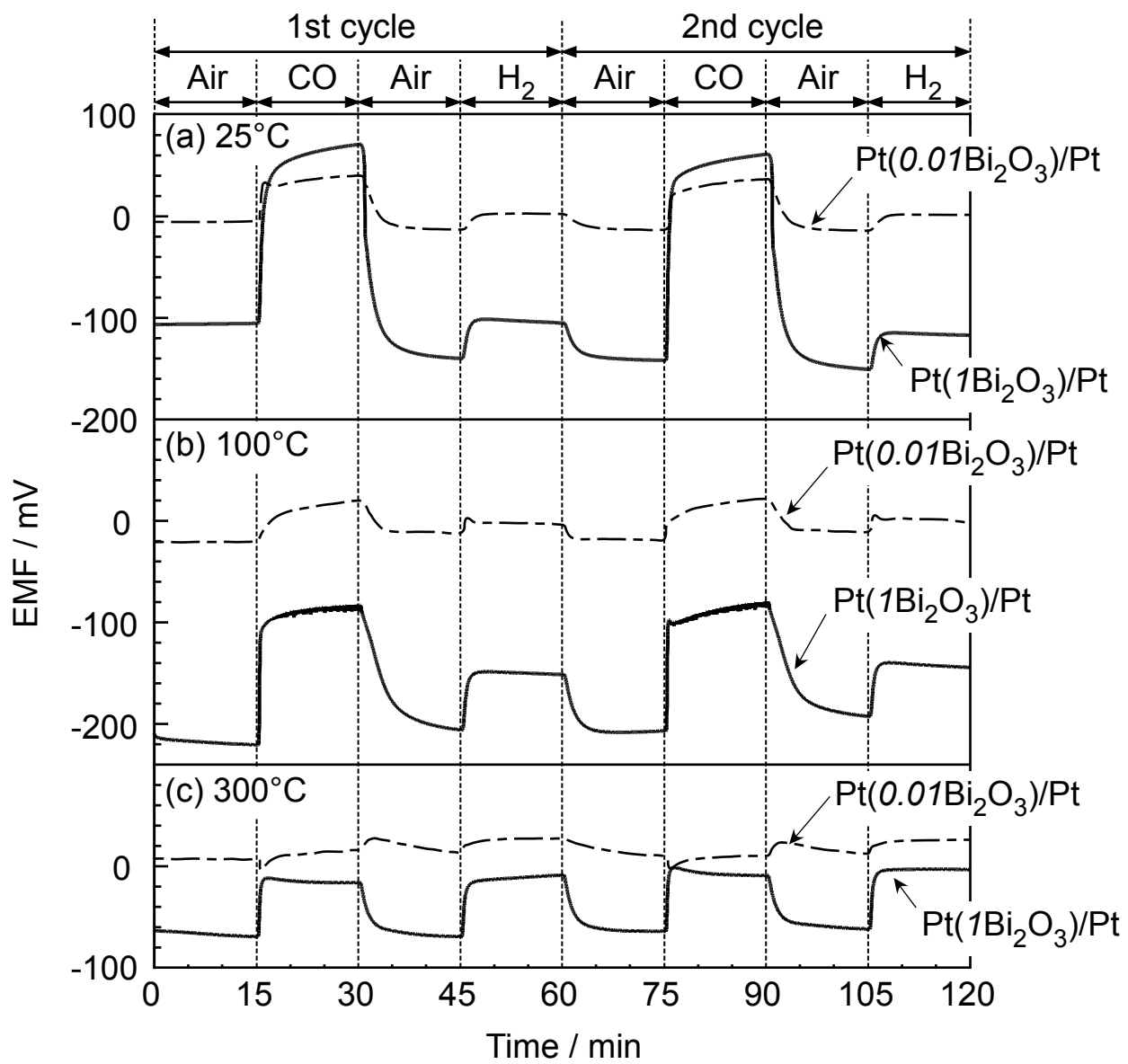


Fig. 9 Takeda et al.

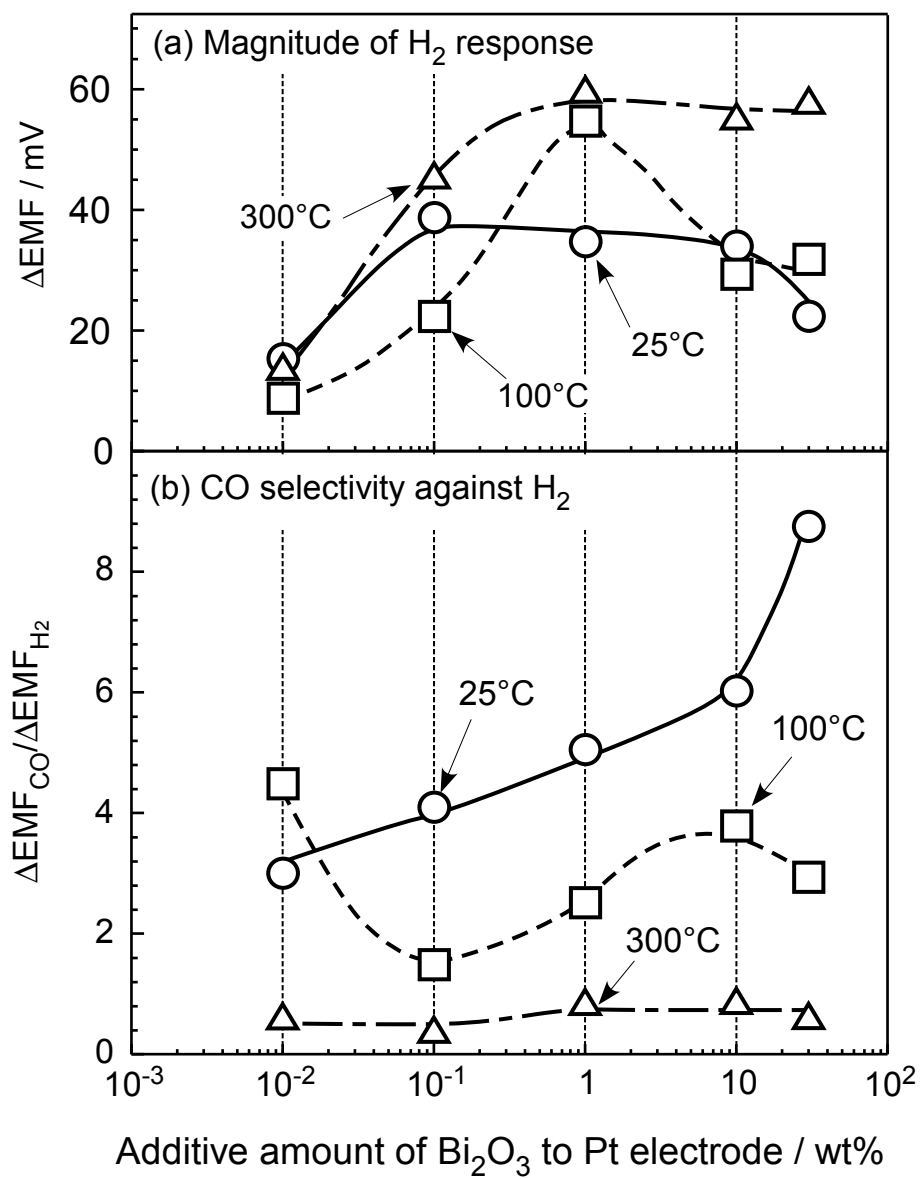


Fig. 10 Takeda et al.

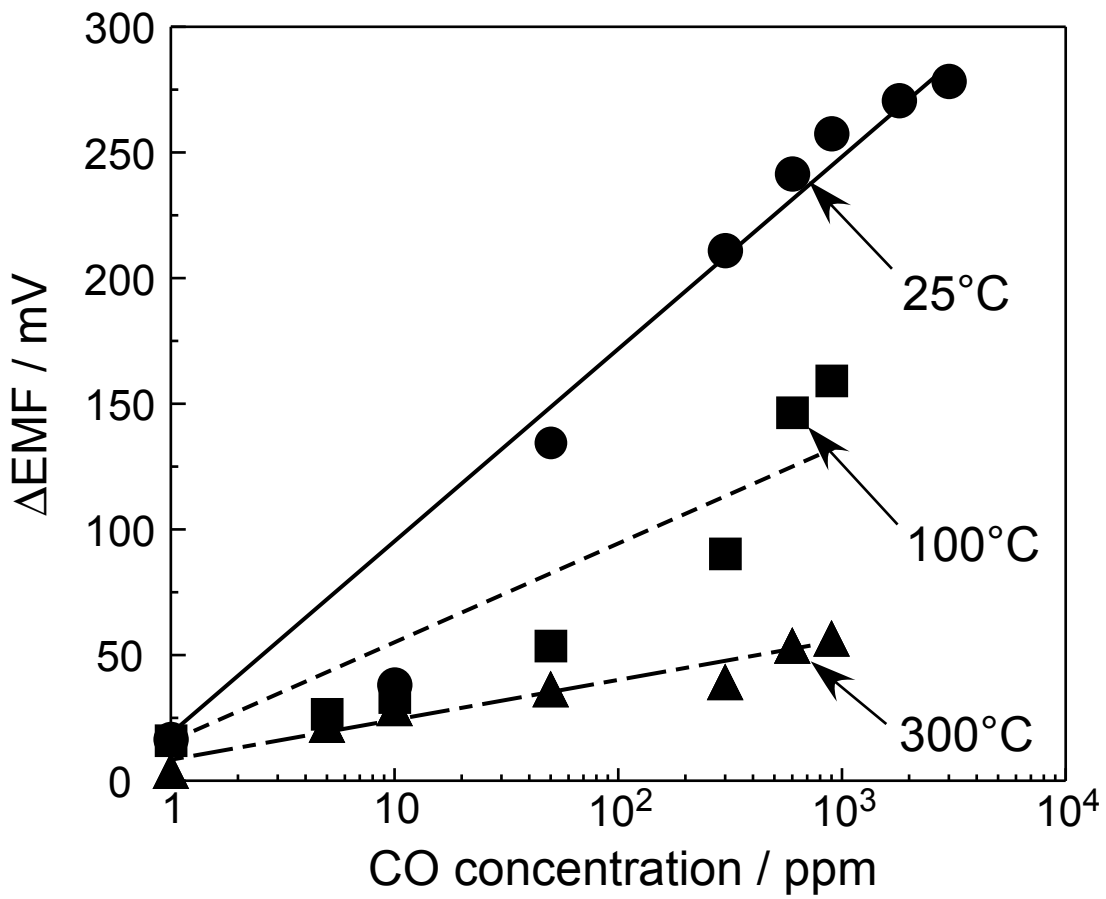


Fig. 11 Takeda et al.

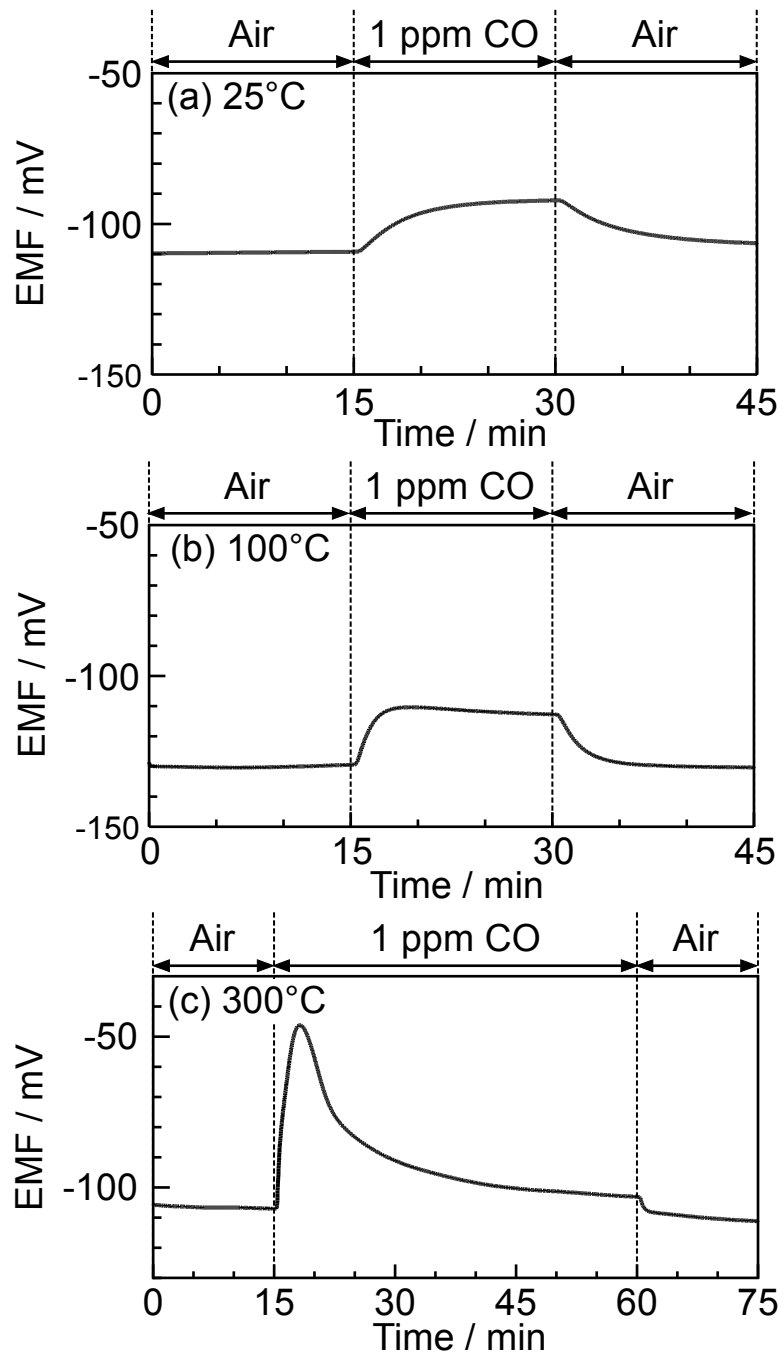
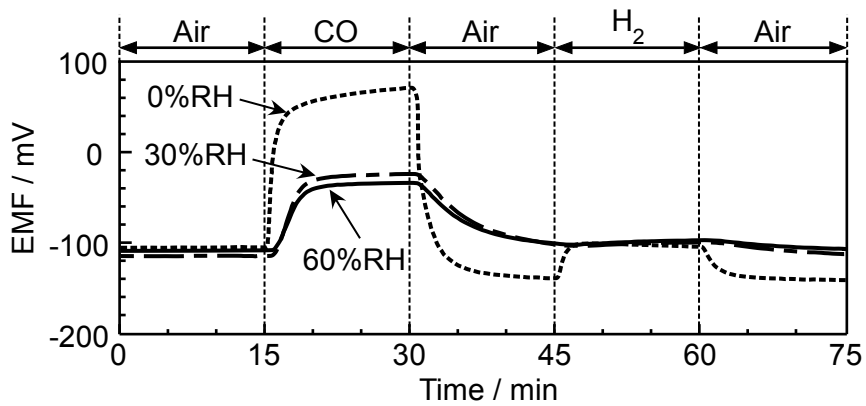


Fig. 12 Takeda et al.

(a) Response transients to 300 ppm CO and H<sub>2</sub>



(b) CO selectivity against H<sub>2</sub>

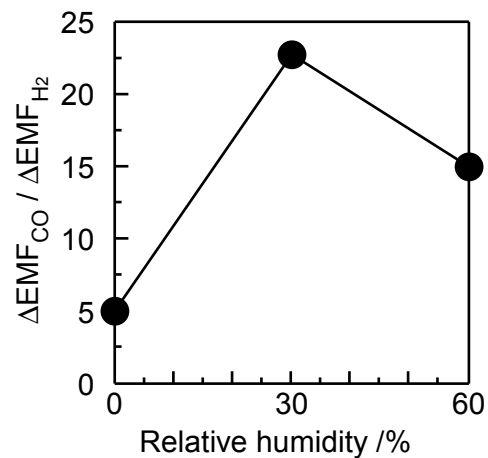


Fig. 13 Takeda et al.

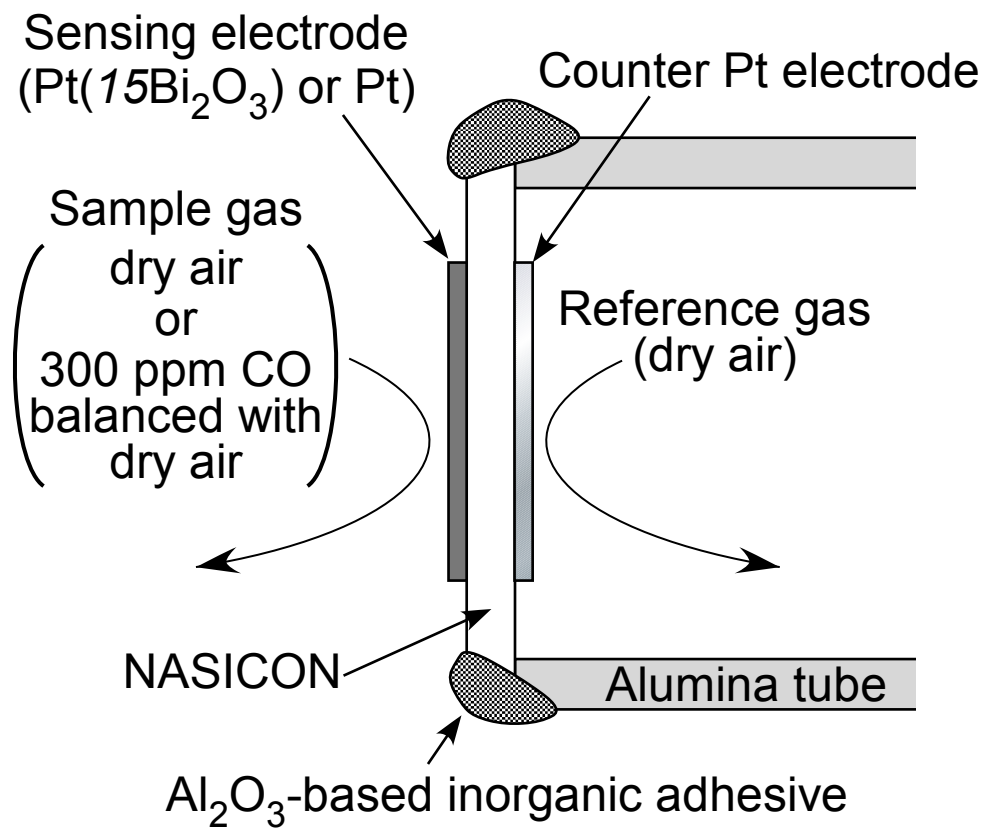


Fig. 14 Takeda et al.

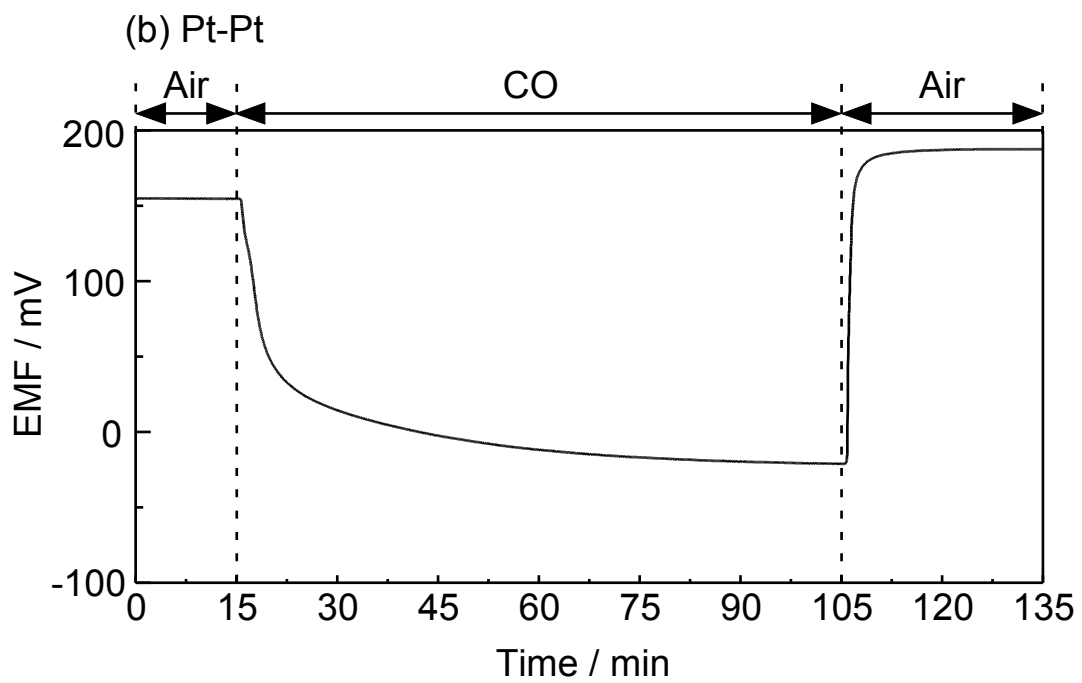
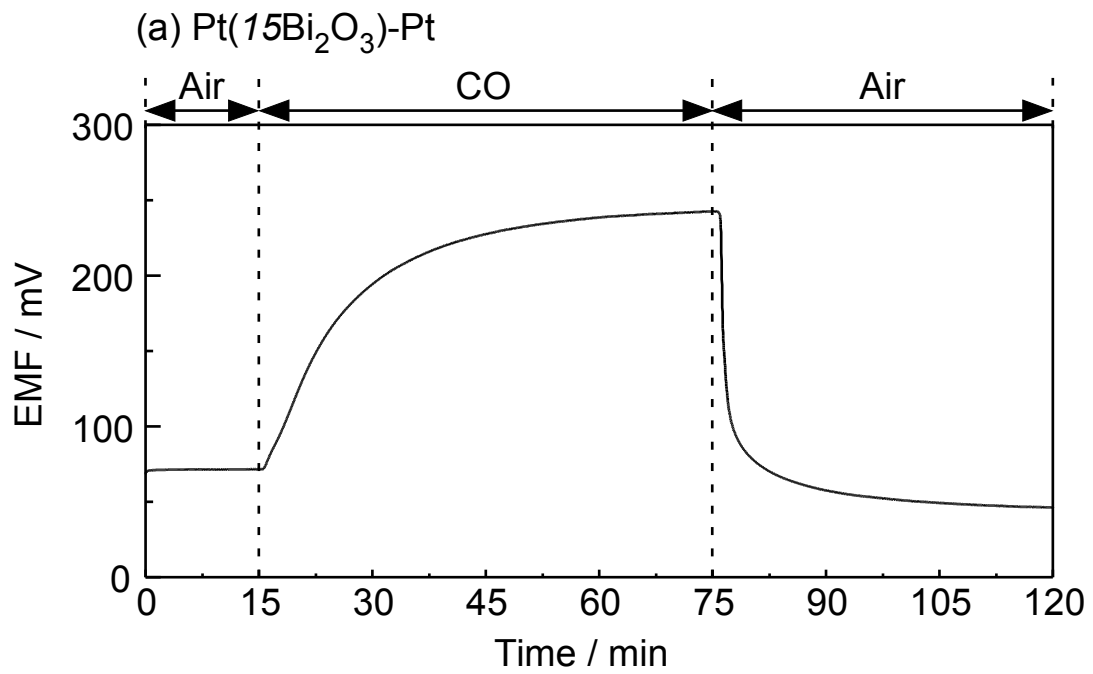


Fig. 15 Takeda et al.

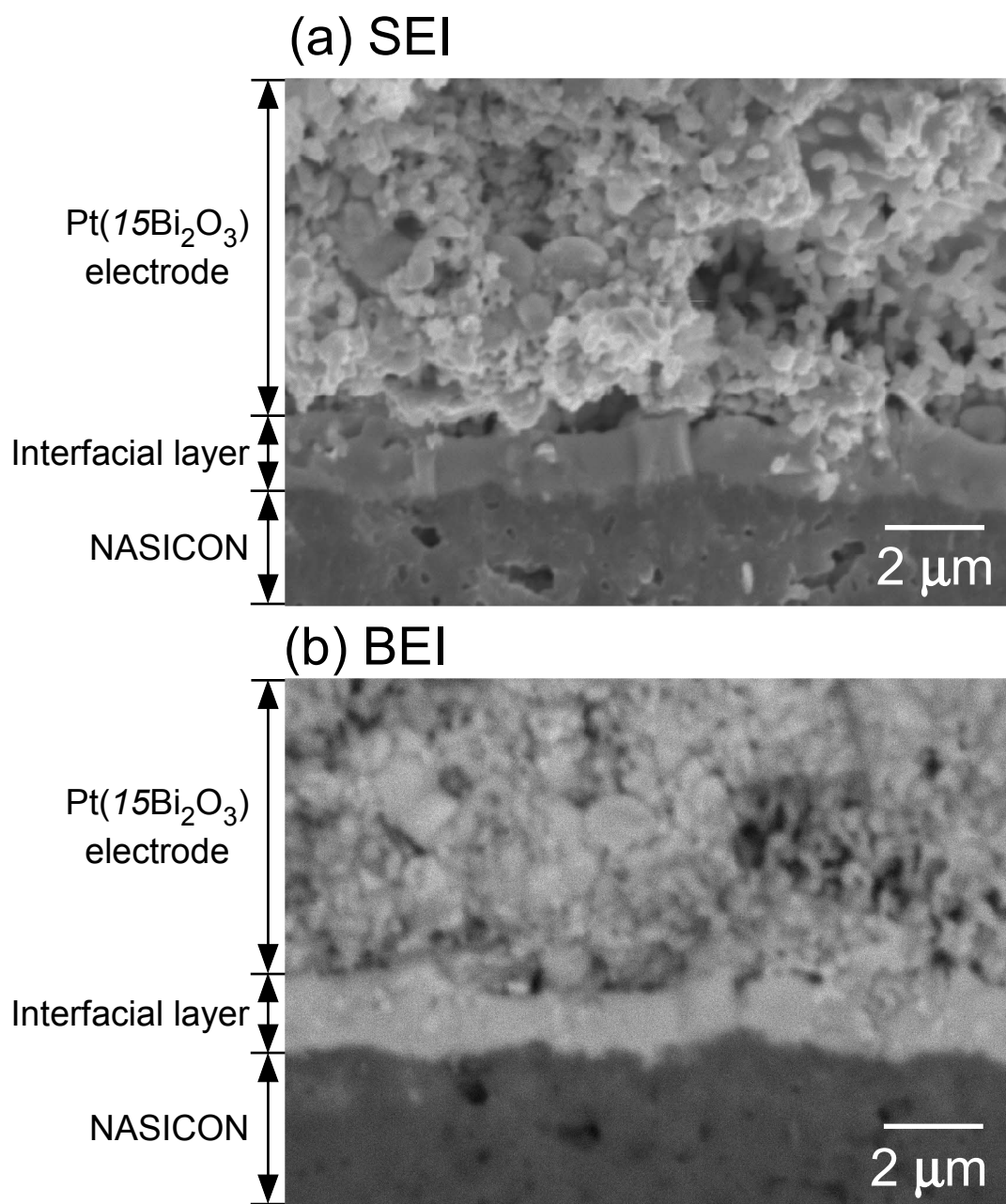


Fig. 16 Takeda et al.

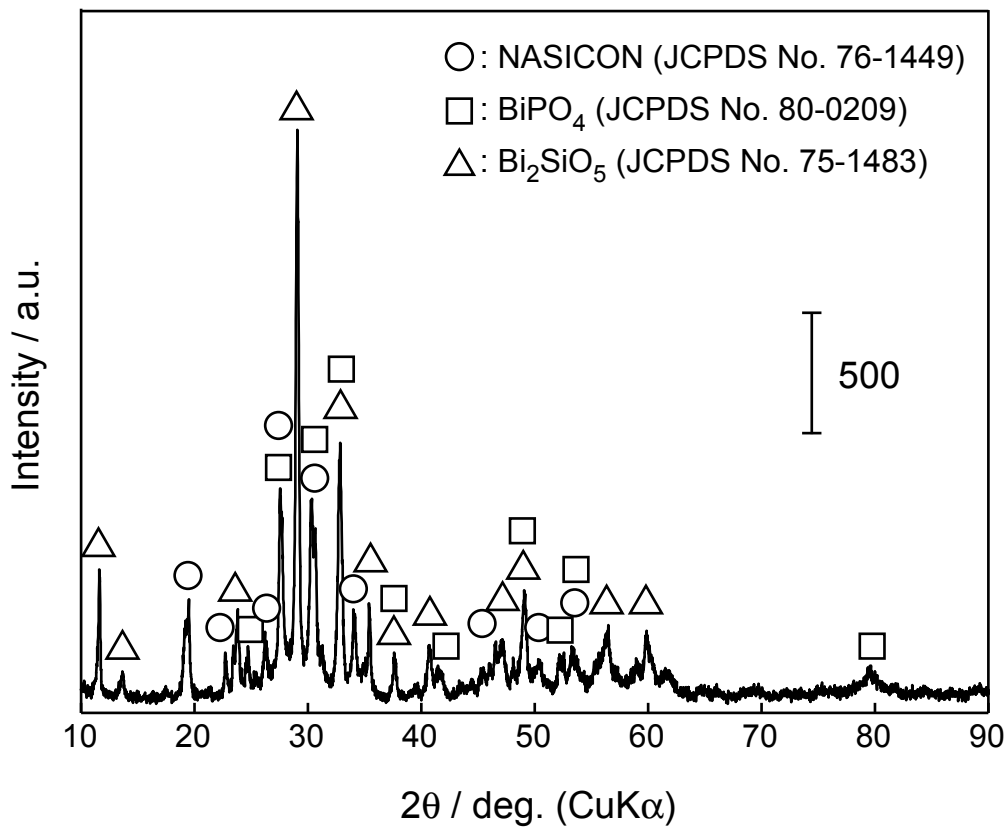


Fig. 17 Takeda et al.